Ellipsometric study of depletion at oil-water interfaces

James P. R. Day and Colin D. Bain*
Department of Chemistry, Durham University, South Road, Durham DH1 3LE, United Kingdom
(Received 7 March 2007; published 5 October 2007)

Ellipsometry is exquisitely sensitive to density variations across a fluid-fluid interface. The coefficient of ellipticity at the interface between water and a series of nonpolar and polar oils is the opposite sign to that predicted for an interface roughened by thermal capillary waves. For pure hydrocarbons, the coefficient of ellipticity is correlated with the refractive index of the oil, but is largely independent of the molecular architecture of the oil phase, ruling out molecular alignment at the interface as the major cause of the deviation from the capillary-wave model. The introduction of a "drying" layer between the oil and water can explain the experimental data. The thickness of the drying layer, modeled as a slab with a relative permittivity of unity, was only 0.3–0.4 Å, which is close to that expected simply from the hard sphere repulsion of a hydrocarbon surface. For polar oils, the coefficient of ellipticity decreases as the interfacial tension decreases, consistent with the reduction in thickness of the hard-sphere exclusion region on account of the formation of hydrogen bonds to water.

DOI: 10.1103/PhysRevE.76.041601 PACS number(s): 68.05.−n, 07.60.Fs, 78.68.+m

I. INTRODUCTION

The density profile at a fluid interface is not a step; the density variation typically occurs over a few molecular diameters as predicted by classical van der Waals theory [1]. At the air-water interface this profile is monotonic. Lum, Chandler, and Weeks have postulated that at the interface between water and a hydrophobic solute, anisotropy in the intermolecular forces may lead to depletion (reduced water density) or accretion (increased water density), depending on the size of the solute [2]. For a planar interface, a depletion or "drying" layer was predicted. In this work, we have employed ellipsometry to investigate density profiles at oil-water interfaces and the effect of the molecular structure of the oil on these profiles.

The nature of the pristine interface between oil and water has been extensively investigated by various experimental techniques, including x-ray [3] and neutron reflection [4], sum-frequency [5,6] and second-harmonic generation [7], and ellipsometry [5,8], as well as by molecular dynamics simulations [9–13]. Nevertheless, the debate in the literature as to the nature of the density profile at the oil-water interface continues [14–16]. Our work was stimulated by the observation that the ellipticity of the hexadecane-water interface is of opposite sign to that expected for a simple, thermally roughened interface. Ellipsometry is exquisitely sensitive to the optical density profile at an interface and, although the interpretation of ellipsometry measurements is model dependent, the reversal of the sign itself suggests that ellipsometry may be a useful tool to investigate the behavior of the mass density profile at the oil-water interface.

In ellipsometry, a polarized light beam is reflected from a surface and the change in the polarization of the light is detected [17]. The coefficient of ellipticity, $\bar{\rho}$, is defined as $\mathrm{Im}(r_p/r_s)$ at the Brewster angle θ_B, where r_p and r_s are the reflection coefficients for *p*- and *s*-polarized light and θ_B is the angle where $\mathrm{Re}(r_p/r_s)=0$. When the thickness of the interfacial region is much less than the wavelength λ of the incident light, a single interfacial parameter η, with dimensions of length and known as the ellipsometric thickness, determines $\bar{\rho}$ [18] as follows:

$$\bar{\rho} = \frac{\pi}{\lambda}\frac{\sqrt{\varepsilon_1+\varepsilon_2}}{(\varepsilon_1-\varepsilon_2)}\eta, \tag{1}$$

where ε_1 and ε_2 are the relative permittivities of oil and water, respectively, at wavelength λ. In the presence of a thin isotropic film, the Drude equation relates η to the permittivity profile normal to the surface [18,19] as follows:

$$\eta = \int \frac{(\varepsilon-\varepsilon_1)(\varepsilon-\varepsilon_2)}{\varepsilon}dz. \tag{2}$$

The Drude equation can also be extended to describe a uniaxial film with different permittivities parallel, ε_o, and perpendicular, ε_e, to the interface [20,21] as follows:

$$\eta = \int \frac{(\varepsilon_e-\varepsilon_1)(\varepsilon_e-\varepsilon_2)}{\varepsilon_e} + (\varepsilon_o-\varepsilon_e)dz. \tag{3}$$

There are two alternative ways to treat thermal roughening of the interface: either as a modulation of the shape of a sharp interface by capillary waves or as a smooth monotonic variation in the density profile between bulk values. In the first instance, coupled-mode theory predicts the roughness contribution to the ellipticity $\bar{\rho}_{r1}$ to be [22]

$$\bar{\rho}_{r1} = -\frac{3\pi(\varepsilon_1-\varepsilon_2)}{2\lambda\sqrt{\varepsilon_1+\varepsilon_2}}\sqrt{\frac{\pi k_B T}{6\gamma_{ow}}}, \tag{4}$$

where γ_{ow} is the interfacial tension. At the air-water surface, $\varepsilon_1<\varepsilon_2$ and Eq. (4) predicts that the ellipticity of the pristine surface is positive. In contrast, for the oil-water interfaces studied in this work, $\varepsilon_1>\varepsilon_2$ and Eq. (4) predicts negative ellipticities. This formula has been used extensively to describe roughening at the air-liquid interface and gives the correct sign and variation with temperature and surface ten-

*Corresponding author. c.d.bain@durham.ac.uk

sion, although it overestimates the ellipticity of the air-water interface by 40% [22]. In the second instance, a suitable functional form is chosen for the density profile normal to the interface and an effective medium approximation (EMA) is used to calculate the permittivity profile. This profile is used in the Drude equation to calculate η. While one can debate the meaning of a local dielectric function on a length scale smaller than that of a molecule, the treatment of ellipsometry in terms of a continuously varying dielectric constant is well established in the literature [23,24]. Lekner has derived Eq. (2) to second order in the interface thickness for an arbitrary dielectric profile [19].

In the Results and Discussion sections, we first present ellipsometric data for a series of nonpolar and polar oils on water. We then use two alternative models to provide a quantitative microscopic description of these results within a simple physical framework. Finally, we place our work into context with other related studies on the oil-water interface.

II. EXPERIMENTAL

A. Materials

Octane (≥99%), tridecane (≥99%), tetradecane (≥99%), hexadecane (≥99%), isooctane (99.8%), squalane (99%), 2,2,4,4,6,8,8-heptamethylnonane (98%), 1,3-dimethyladamantane (DMA) (≥99%), *cis*-decalin (99%), *trans*-decalin (99%), toluene (≥99.9%), 1,2,3,4-tetrahydronaphthalene (99%), squalene (≥98%), dibutyl ether (99.3%), 5-nonanone (98%), cyclohexylacetate (99%), ethyl acetate (99.8%), and 3-pentanone (≥99%) were purchased from Aldrich. Butyl butanoate (≥99%) and 5-nonanol (≥99.5%) were purchased from Fluka. All oils were purified by passing three times through a column of activated neutral alumina. The purity of the alkanes was checked by a Zisman test [25]. A small drop of the oil was placed on the surface of acidic (pH <4) and basic (pH >10) aqueous solutions and the flasks covered with a watch glass to limit evaporation. The oil was classed as pure if the drop did not spread over a period of several hours. To check the purity of the other oils, the oil-water interfacial tension was monitored as a function of time—for all the oils, the time-averaged interfacial tension varied by less than 0.1 mN m^{-1} over ten minutes. Interfacial tensions were measured at 293 K by axisymmetric drop shape analysis (FTA200, First Ten Ångstroms) on a rising bubble of oil in water. Polar oils with appreciable mutual solubility with water were shaken with water and stored in contact with water overnight to equilibrate. Ultrahigh purity (UHP) water from a Millipore MilliQ system was used throughout. Glassware and the ellipsometry cell were cleaned by sonication in alkaline detergent (Decon 90) followed by rinsing in UHP water, sonication in acetone, thorough rinsing in UHP water, and finally drying in a stream of dry air.

B. Ellipsometry and ellipsometry cell

The phase modulation ellipsometer (Beaglehole Instruments, Wellington, NZ) has been described in detail previously [26]. The ellipsometry cell was based on a design by Benjamins [27] to ensure a planar interface between the oil and water phases. The cross section of the cell is shown in Fig. 1.

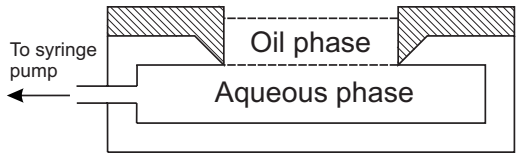

FIG. 1. Cross section of the ellipsometry cell. The hatched region is manufactured from Teflon and the white region from stainless steel. Not to scale.

The stainless steel body of the cell has an overhanging lip and is capped by a tight-fitting Teflon ring, so that the interface is pinned at the steel-Teflon intersection. The aqueous phase was introduced into the stainless steel body from a 5 ml gas-tight syringe (Hamilton, Reno, NV) via a sidearm and the precise volume was controlled by an 11 Plus infuse-withdraw syringe pump (Harvard Apparatus, Holliston, MA). The cell was filled with water to the bottom of the overhanging lip, and the oil phase was introduced on top with a pipette. The volume of the aqueous phase was adjusted until the reflected laser beam had a circular cross section, indicative of a planar interface. The laser beam passed through two light guides immersed in the oil phase, as described by Benjamins [27]. The guides were constructed from 5 mm o.d. nuclear magnetic (NMR) tubes with their ends ground flat and glued to sections of optical microscopy coverslips with Araldite. The coefficient of ellipticity of pure water in the cell was measured to check the cleanliness of the cell. The effect of the light guides on the ellipticity was determined in the same way. In both cases, $\bar{\rho}=(3.8\pm0.3)\times10^{-4}$, a typical level of experimental precision for this ellipsometer. The ellipticity of each oil-water interface was measured three times for two minutes at a time. The cell was then cleaned and reassembled and the procedure repeated for the same oil twice more, giving a total of three sets of three readings for each oil. All experiments were performed at room temperature (293 K).

III. RESULTS

Figure 2 displays the coefficients of ellipticity $\bar{\rho}$ measured for the linear alkanes (■), as a function of the refractive index of the oil phase $n_1=\sqrt{\varepsilon_1}$, given in Table I. We calculated the expected contribution to $\bar{\rho}$ from thermal roughening with Eq. (4), the values of n_1 in Table I and a value of ε_2 for water of 1.774; these values are shown in Fig. 2 as open circles (○). It is immediately evident that the simple picture of a sharp interface between two homogeneous bulk phases roughened by capillary waves does not explain the experimental results: not even the sign of $\bar{\rho}$ is correct. A positive value of $\bar{\rho}$ can conceivably arise from three sources: alignment of molecules, a dip in the density profile in the aqueous phase, or a peak in the density profile of the oil phase. Molecular dynamic simulations often predict oscillations in the water and oil densities at the interface [10,12,13]. These os-

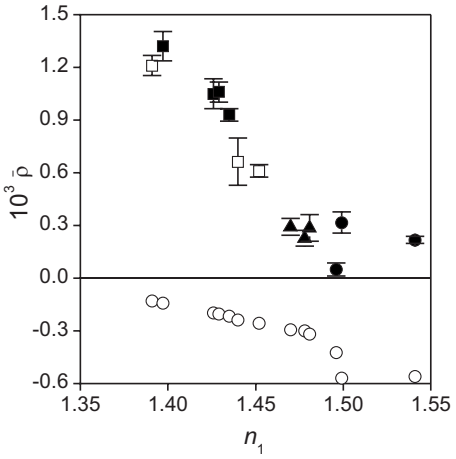

FIG. 2. Coefficient of ellipticity $\bar{\rho}$ of the oil-water interface as a function of the refractive index of the oil phase n_1 for a series of linear alkanes (■), branched alkanes (□), cyclic alkanes (▲), and unsaturated oils (●). The expected roughness contribution from coupled-mode capillary wave theory is also shown for each oil (○).

cillations arise from packing effects and vary around a mean density. Ellipsometry is not sensitive to the oscillations themselves, only to the mean density upon which the oscillations are superimposed.

To assess the possible role of anisotropy in yielding positive values of $\bar{\rho}$ for alkanes, we selected a series of hydrocarbons with different molecular architectures. Anisotropy in the refractive indices of a uniaxial linear alkane film arises from the difference in the polarizability of these molecules along and perpendicular to the principal molecular axis.

If hydrocarbon chains were to have a preferential alignment normal to the interface, then ε_e would be greater than ε_o and the ellipticity would be negative. For chains lying parallel to the interface, $\varepsilon_o > \varepsilon_e$, resulting in a positive contribution to $\bar{\rho}$. Branched or cyclic alkanes exhibit a more nearly spherical polarizability ellipsoid, hence if the positive ellipticity of linear alkanes is caused by a uniaxial film at the interface, we should see a reduction in the ellipticity for cyclic and branched alkanes. The measured ellipticities for a series of cyclic (▲) and branched alkanes (□) are plotted in Fig. 2. Although the absolute magnitude of the ellipticity for most of these oils is lower than for the linear alkanes, all the data fall on the same line when plotted against the refractive index of the oil phase (*vide infra*). To assess the effect of architecture, it is instructive to consider two pairs of oils. First, the structural isomers octane and isooctane have very similar refractive indices and ellipticities that differ by less than 1×10^{-4}. For heptamethylnonane and hexadecane again with similar refractive indices—the variation in ellipticity is slightly larger, but still less than 3×10^{-4}. The close agreement between the linear and highly branched alkanes suggests that anisotropy is not the major factor determining the positive ellipticities. Indeed, the ellipticity for 1,3-dimethyladamantane (DMA) is still positive, despite the fact that this molecule is nearly spherical and hence is unable to form an optically anisotropic layer at the interface. We have also measured $\bar{\rho}$ for the interfaces between pure water and two aromatic oils and one olefin (●). All three of these oils give small positive values for $\bar{\rho}$; the behavior is not dramatically different from the saturated alkanes (Fig. 2).

If the origin of the positive ellipticity for the simple hydrocarbon-water interface is related to the hydrophobicity of the interface then we expect that increasing the polarity of the oil phase will cause the ellipticity of the interface to approach the capillary-wave prediction. To test this hypothesis, we measured the ellipticity for a series of alkanes functionalized with polar ether, ketone, and ester groups (Table III). As ellipsometry is so sensitive to anisotropy at the interface, we have chosen molecules that are not potentially amphiphilic. We plot $\bar{\rho}$ for these compounds as a function of n_1 in Fig. 3(A) and as a function of interfacial tension γ_{ow} in Fig. 3(B); the datum for hexadecane is included in the plots for comparison.

There is no correlation between $\bar{\rho}$ and n_1 for these oils [Fig. 3(A)], in contrast to nonpolar hydrocarbons in Fig. 2. For polar oils, the mutual solubility of the oil and water phases is no longer negligible and the formation of two mixed bulk phases, one rich in oil and one rich in water, alters the refractive indices relative to the pure liquids. The relative permittivities of these solutions can be approximated by the Lorentz-Lorenz effective medium approximation [28] as follows:

$$\left(\frac{\varepsilon-1}{\varepsilon+2}\right) = \varphi_1\left(\frac{\varepsilon_1-1}{\varepsilon_1+2}\right) + \varphi_2\left(\frac{\varepsilon_2-1}{\varepsilon_2+2}\right), \tag{5}$$

where ε is the permittivity of the mixed phase and φ_1 and φ_2 are the volume fractions of oil and water, respectively, such

TABLE I. Refractive index n_1, coefficient of ellipticity $\bar{\rho}$, interfacial tension γ_{ow}, and roughness contribution to ellipticity [Eq. (4)], $\bar{\rho}_{r1}$, for a series of nonpolar oils. n_1 is given for $\lambda = 589$ nm, whereas the ellipsometer uses a HeNe laser at 633 nm; none of the oils have significant dispersion at visible wavelengths.

Oil	n_1	$10^3\bar{\rho}$	γ_{ow} (mN m^{-1})	$10^3\bar{\rho}_{r1}$
Octane	1.397[a]	1.32	51.7[e]	−0.14
Tridecane	1.426[a]	1.05	52.2[f]	−0.20
Tetradecane	1.429[a]	1.06	53.3[e]	−0.21
Hexadecane	1.435[a]	0.93	53.8[e]	−0.22
Isooctane	1.391[b]	1.21	49.3[g]	−0.13
Heptamethylnonane	1.440[c]	0.66	48.8[f]	−0.24
Squalane	1.452[a]	0.61	52.3[h]	−0.26
trans-Decalin	1.470[a]	0.29	51.4[e]	−0.30
DMA	1.478[d]	0.23	56.7[f]	−0.30
cis-Decalin	1.481[a]	0.29	51.7[e]	−0.32
Toluene	1.496[a]	0.05	35.7[g]	−0.42
Tetrahydronapthalene	1.541[a]	0.22	33.0[f]	−0.56
Squalene	1.499[a]	0.32	20.3[f]	−0.57

[a]Reference [43].
[b]Reference [44].
[c]Reference [45].
[d]Reference [46].
[e]Reference [47].
[f]This work.
[g]Reference [48].
[h]Reference [49].

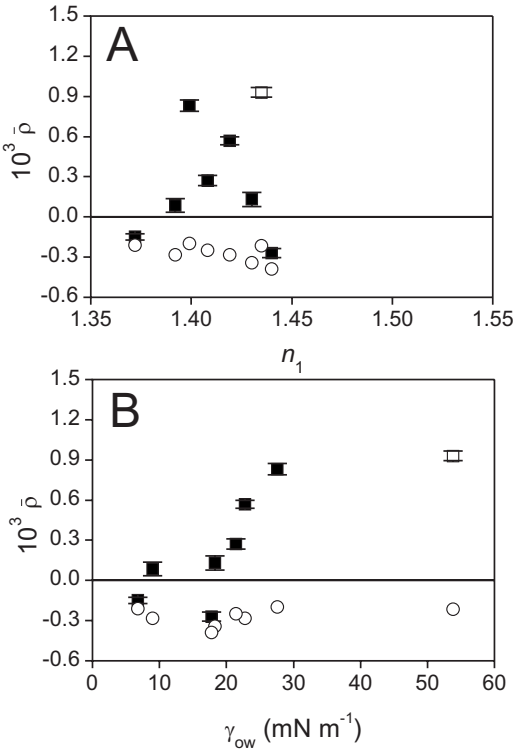

FIG. 3. (A) Coefficient of ellipticity $\bar{\rho}$ of the oil-water interface as a function of the refractive index of the oil phase n_1 for a series of polar oils (■) and hexadecane (□). The expected roughness contribution from coupled-mode capillary-wave theory is also shown for each oil (○). (B) The same data plotted as a function of the interfacial tension γ_{ow}.

that $\varphi_1+\varphi_2=1$. The mutual solubilities and the calculated refractive indices of the adjoining phases are given in Table II. The mutual solubility has a small effect on the refractive indices of the ethyl acetate, 3-pentanone and 5-nonanol systems, and a negligible effect on all other systems. We also plot the capillary wave prediction for each interface in Fig. 3 using the data from Table III. Figure 3(B) shows that as the interfacial tension decreases, the values of $\bar{\rho}$ approach the capillary-wave prediction.

TABLE III. Measured ellipticity $\bar{\rho}$, interfacial tension γ_{ow}, and contribution to ellipticity from thermal roughening $\bar{\rho}_{r1}$ for a series of polar oils.

Oil	$10^3\bar{\rho}$	γ_{ow} (mN m^{-1})	$10^3\bar{\rho}_{r1}$
Ethyl acetate	−0.15	6.80	−0.21
3-Pentanone	0.09	9.00	−0.29
Dibutylether	0.83	27.6	−0.20
Butyl Butanoate	0.27	21.4	−0.25
5-Nonanone	0.57	22.8	−0.28
5-Nonanol	0.13	18.3	−0.35
Cyclohexyl acetate	−0.15	17.8	−0.39

IV. DISCUSSION

Ellipsometry of an oil-water interface yields only a single independent parameter: the ellipsometric thickness η. Given that η is a function of the roughness of the interface as well as the refractive index, thickness, and anisotropy of any structured layer at the interface, it might at first sight appear that to attempt an interpretation of ellipsometry in terms of a physical model of the interfaces is futile. For the oil-water interface, however, we have established experimentally that optical anisotropy alone cannot describe our results and that the measured ellipticity differs from the capillary wave prediction not merely in magnitude but in sign. With the aid of some simple assumptions, it is possible to derive useful physical insights. To proceed with our model building, we first describe two alternative formalisms for calculating the contribution of thermal roughening to the ellipticity and then use these formalisms to evaluate the extent of any depletion layer at the interface between oil and water. In the notation of Mecke and Dietrich [29], model 1 is similar to the Buff, Lovett, and Stillinger (BLS) approach, where the interfacial profile is considered as a steplike interface roughened by thermally excited capillary waves. Model 2 is related to the approach of van der Waals where the density profile normal to the interface varies smoothly between the two phases. While these two models are, in principle, equivalent, they make different assumptions about the nature of the interface

TABLE II. Refractive index of pure oil phase n_1, mutual solubility and adjusted refractive indices of the water n_{water}, and oil n_{oil} phases for a series of polar oils.

Oil	n_1	Solubility of water in oil (wt %)	Solubility of oil in water (wt %)	n_{water}	n_{oil}
Ethyl acetate	1.372	2.88	7.79	1.335	1.371
3-Pentanone	1.392	2.00	5.30	1.336	1.391
Dibutyl ether	1.399	0.27	0.02	1.332	1.399
Butyl butanoate	1.408	0.44	0.07	1.332	1.408
5-Nonanone	1.420	0.44	0.05	1.332	1.420
5-Nonanol[a]	1.430	3.14[b]	0.04	1.332	1.427
Cyclohexyl acetate	1.440	0.71	0.30	1.332	1.439

[a]In the absence of mutual solubility data for 5-nonanol, data for 2-nonanol have been used.
[b]Reference [50].

on a molecular length scale. It is therefore instructive to interpret the ellipsometric results within both conceptual frameworks.

A. Model 1

A sharp interface is modulated by capillary waves and coupled-mode theory is used to arrive at Eq. (4). Local structure at the interface is treated by a stratified-layer model and the Drude equation used to determine the ellipsometric thickness. The contributions to $\bar{\rho}$ from the roughness and local structure are then summed [22]. We first consider the case where the positive ellipticity of a hydrocarbon-water interface arises from a thin layer of structured, icelike water at the interface. To estimate the refractive index of the icelike layer, we employ the Clausius-Mossotti equation in the form

$$\left(\frac{\varepsilon-1}{\varepsilon+2}\right)\frac{1}{\rho}=\text{constant}, \tag{6}$$

where ρ is the density. Using a value for the density of ice of 0.917 g cm^{-3} [30], the refractive index of ice at 293 K is 1.303. Taking the hexadecane-water interface as a typical example, the layer of icelike water between the bulk phases would have to be ~21 Å thick to explain the measured ellipticity. An intermediate structure between bulk ice and water would be even thicker. Such a thick layer at the interface would be clearly manifested in x-ray reflectivity if it existed: no such layer has been observed [3].

We next consider a denser oil phase at the interface with the same protocol described above and taking the hexadecane-water interface as a representative example. The density of solid hexadecane is 0.926 g cm^{-3} [31]. From the Lorentz-Lorenz relationship, the (isotropic) refractive index of a solid layer would be 1.537 and the layer would have to be ~5 Å thick to describe the measured ellipticity. Crystalline hydrocarbons are, however, optically anisotropic and it is known from ellipsometric studies of surface freezing at the oil-water interface that the anisotropic contribution to the ellipticity is larger than the isotropic contribution [32]. While it is possible that the effects of the increased density and anisotropy are balanced so perfectly that branched and linear alkanes behave alike ellipsometrically, such a serendipitous outcome is very unlikely. A small increase in density of an alkane might be accommodated without pronounced anisotropy, but then the region of increased density increase would have to extend implausibly far into the bulk oil phase. Hence we conclude that densification of the oil at the interface is unlikely to be the origin of the positive ellipticity.

Finally, we consider the case where the hydrophobic interface leads to a depleted water layer of greatly reduced density at the interface, as depicted in Fig. 4—a situation known as "drying."

In the limit of total drying, this depletion layer will have a refractive index of unity. After accounting for the capillary-wave contribution, we calculate the thickness of the depletion layer d that would generate the experimental ellipticity for each oil. These thicknesses are plotted as a function of interfacial tension in Fig. 5. The absolute values of d are extremely small—all are less than 0.5 Å.

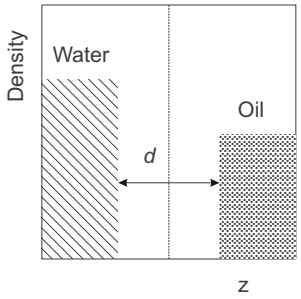

FIG. 4. Density profile through the interface for model 1. z is the coordinate normal to the interface.

To understand why a density gap of this magnitude arises, it is instructive to compare d with the gap between layers in orthorhombic crystals of long-chain, odd-numbered, linear alkanes. In Fig. 6, we plot the c lattice parameter (along the chain axis) of the crystal unit cell as a function of chain length: the intercept is 3.6 Å.

This nonzero intercept arises because the van der Waals diameter of a methyl group is much larger than the methylene repeat distance (1.27 Å). The region between the terminal methyl groups of two adjacent layers is sketched in Fig. 7. Since the unit cell contains two layers of alkanes, the "gap" between layers is 1.8 Å, or 0.9 Å per surface. The electron density of the terminal hydrogen of the methyl group is much less than that of a methylene group. Consequently, for a truncated crystalline alkane next to a water surface, we would expect a deficit in the electron density corresponding to a ~0.9 Å void, purely due to the excluded volume of the terminal methyl group—even without any structuring of the interfacial water.

The effect of the terminal methyl groups on ellipsometry is more complicated than on x-ray reflectivity since the polarizability of the terminal C-H bond is not negligible compared to a methylene group; consequently, the "polarizability deficit" will be smaller than the electron density deficit at the interface. Nevertheless, the excluded volume of the methyl

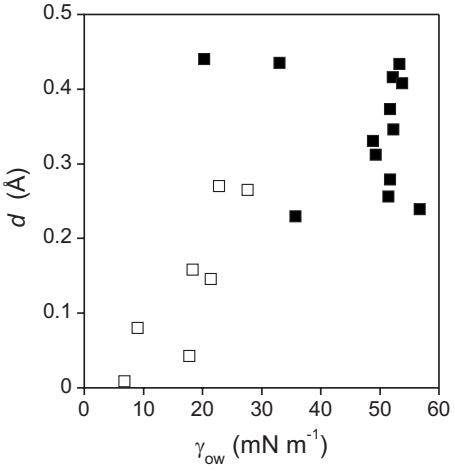

FIG. 5. Thickness of depleted layer determined using model 1, d, as a function of interfacial tension γ_{ow} for a series of polar (□) and nonpolar (■) oils.

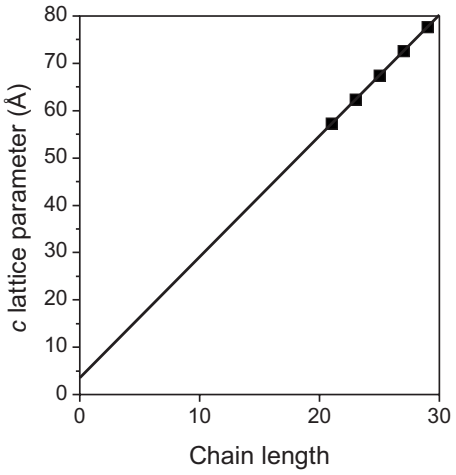

FIG. 6. c lattice parameter of orthorhombic alkanes plotted against chain length. Data taken from D. E. Small, *The Physical Chemistry of Lipids* (Plenum, New York, 1985).

group still results in a region of reduced polarizability compared to the hydrocarbon chains. To quantify this effect, we treat the methyl group as having a thickness $L[CH_3]$ of equal polarizability density to that of a methylene group. The "gap" d_α sensed by ellipsometry is then given by

$$d_\alpha = 0.9 + L[CH_2] - L[CH_3], \tag{7}$$

where $L[CH_2]=1.27$ Å is the CH_2 repeat length from crystallographic studies (see Fig. 7). $L[CH_3]$ can be expressed in terms of the molar refractivities R_m of methyl and methylene groups by

$$L[CH_3] = L[CH_2] \times R_m[CH_3]/R_m[CH_2]. \tag{8}$$

R_m is an additive property that is related to the polarizability volume α' by the relationship $R_m = 4\pi\alpha' N_A/3$, where N_A is Avogadro's number. We determine R_m for methyl and methylene groups from the bond refractivities of C-C bonds (1.20 $cm^3\ mol^{-1}$) [33] and C-H bonds (1.65 $cm^3\ mol^{-1}$) [33] to give $R_m[CH_3]=5.55\ cm^3\ mol^{-1}$ and $R_m[CH_2]=4.50\ cm^3\ mol^{-1}$. Hence $L[CH_3]=1.57$ Å and $d_\alpha=0.6$ Å, only slightly larger than the value of d we deduce from ellipsometric measurements on the simple hydrocarbons. We are, of course, studying liquid hydrocarbons that do not expose an oriented layer of methyl groups at the oil-water interface. Nevertheless, we expect the excluded volume effect of methylene groups to be similar to that of methyl groups and so the polarizability gap for a liquid hydrocarbon will not be much smaller than the value of d_α calculated for crystalline alkanes.

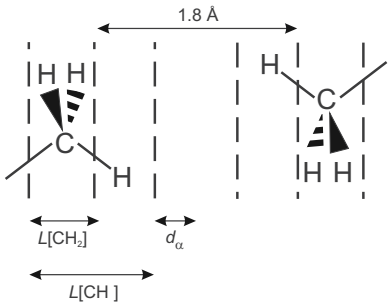

FIG. 7. Schematic showing the polarizability gap d_α, expected between a truncated alkane crystal and water.

For the alkanes, alkene, and aromatics the density profiles show regions of reduced polarizability density of similar magnitudes, but these deficits decrease for the polar oils. The oxygenated functional groups of these oils can form hydrogen bonds with water molecules at the interface, reducing the excluded volume between the oil and the water. Hydrogen bonding between the polar oils and the water is one of the primary reasons for the reduction in interfacial tension: the lower the interfacial tension, the more hydrogen bonds and the smaller the value of d. The interfacial tension is not solely dependent on hydrogen bonding and hence the correlation between γ_{ow} and d is not perfect. For oils with π systems (squalene, toluene, and tetrahydronaphthalene) the greater polarizability of the π electrons reduces the interfacial tension due to dipole-induced dipole interactions, without having a measurable effect on d compared to the saturated hydrocarbons.

B. Model 2

In the second model we consider, we specify the density profiles of both phases at the interface. Following the formalism of Senapati and Berkowitz, the density profiles of the two phases are expressed as [13]

$$\rho_1(z) = \frac{1}{2}\rho_1\left[1 - \mathrm{erf}\left(\frac{z - w_0}{\sqrt{2}w_c}\right)\right],$$

$$\rho_2(z) = \frac{1}{2}\rho_2\left[1 + \mathrm{erf}\left(\frac{z}{\sqrt{2}w_c}\right)\right], \tag{9}$$

where ρ_1 and ρ_2 are the densities of the bulk phases, z is the coordinate normal to the interface, w_c is the width of the interface due to thermal roughening, and w_0 defines the relative positions of the midpoints in the oil and water distributions. w_0 is the parameter that characterizes the extent of interfacial drying. Density profiles derived from model 2 are shown in Figs. 8(A) and 8(B) for $w_0=0$ and $w_0=w_c$, respectively.

w_c is typically derived from the capillary wave theory of independent waves and is given by [1]

$$w_c^2 = \frac{k_B T}{2\pi\gamma}\ln\left(\frac{L_{\max}}{L_{\min}}\right), \tag{10a}$$

where $L_{\max}$ and $L_{\min}$ are related to the longest and shortest wavelength capillary waves that the interface can support. However, to maintain consistency with model 1, we use an alternative expression for w_c based on the coupled-mode theory of Meunier [22]. This approach has the added advantage that the cutoff $L_{\min}$ arises naturally in coupled-mode theory, reducing the number of fitting parameters. From the derivation in the Appendix , w_c is given by

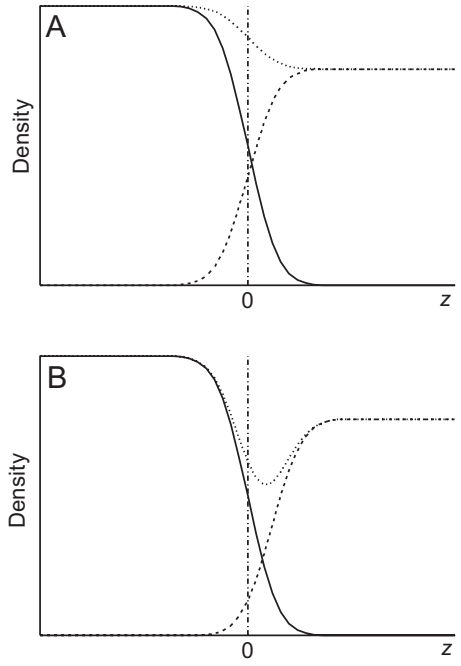

FIG. 8. (A) Model 2 density profile, $w_0=0$. (B) Model 2 density profile, $w_0>0$; $w_0/w_c=1$. (Solid line) water density, (dashed line) oil density, (dotted line) total density, and (dash-dotted line) $z=0$.

$$w_c^2 = \frac{k_B T}{4\pi\gamma} \ln\left(\frac{2\gamma\lambda^2}{3\pi k_B T}\right). \tag{10b}$$

At fixed T and λ, the value of w_c [Eq. (10b)] depends only on the interfacial tension, in an analogous manner to Eq. (4). We use the density profile from Eq. (9) in conjunction with the Lorentz-Lorenz EMA [Eq. (5)] to determine the optical profile across the interface, and finally calculate the ellipticity from the Drude equation [Eq. (2)]. When $w_0=0$, the density profile corresponds to a simple interface roughened by capillary waves and we expect the calculated ellipticity $\bar{\rho}_{r2}$ to be similar to the value for the roughness calculated from Eq. (4) (model 1). We compare the contribution of the roughness to the ellipticity from model 1 and model 2 in Table IV—for most liquids the predictions are in quantitative agreement and the largest deviation is 4×10^{-5}, which is close to the experimental precision.

The values of w_0 required to fit the experimental values of $\bar{\rho}$ are given in Table IV and plotted in Fig. 9. We note two points about the results from model 2. First, the values of w_0 from model 2 vary from 0.5–3 Å and are substantially larger than the values of d from model 1. Although w_0 introduces a separation between the phases akin to d in model 1, the intermediate layer has a refractive index much closer to those of the bulk phases and therefore a value of w_0 larger than d is required to generate the same ellipticity [see Eq. (2)]. Second, the correlation between w_0 and γ_{ow} in Fig. 9 is less apparent than that between d and γ_{ow} in Fig. 5. In model 2, w_0 and w_c are coupled by Eq. (9). A dip in the permittivity profile—which is an essential requirement in the Drude model for a positive ellipticity—only occurs for values of $w_0/w_c>0.1$. The lower the interfacial tension, the rougher the interface and hence the larger the value of w_0 that is required in this model to generate a layer of depleted density at the interface.

TABLE IV. Capillary-wave thickness w_c, roughness contributions to ellipticity calculated by model 1, $\bar{\rho}_{r1}$, and model 2, $\bar{\rho}_{r2}$, depletion layer thickness d, and separation between oil and water phases w_0 for a series of nonpolar and polar oils.

Oil	w_c (Å)	$10^3\bar{\rho}_{r1}$	$10^3\bar{\rho}_{r2}$	d (Å)	w_0 (Å)
Octane	3.0	−0.14	−0.15	0.37	2.1
Tridecane	3.0	−0.20	−0.21	0.42	2.3
Tetradecane	2.9	−0.21	−0.22	0.43	2.3
Hexadecane	2.9	−0.22	−0.23	0.41	2.2
Isooctane	3.0	−0.13	−0.14	0.31	2.0
Heptamethylnonane	3.0	−0.24	−0.25	0.33	2.1
Squalane	3.0	−0.26	−0.28	0.35	2.1
trans-Decalin	3.0	−0.30	−0.32	0.26	1.8
DMA	2.8	−0.30	−0.32	0.24	1.7
cis-Decalin	3.0	−0.32	−0.34	0.28	1.9
Toluene	3.5	−0.42	−0.45	0.23	1.9
Tetrahydronapthalene	3.7	−0.56	−0.60	0.44	2.6
Squalene	4.6	−0.57	−0.58	0.42	2.9
Ethyl acetate	7.6	−0.21	−0.21	0.01	0.5
3-Pentanone	6.6	−0.29	−0.28	0.08	1.5
Dibutylether	4.0	−0.20	−0.21	0.27	2.1
Butyl butanoate	4.5	−0.25	−0.26	0.15	1.7
5-Nonanone	4.3	−0.28	−0.29	0.27	2.2
5-Nonanol	4.8	−0.35	−0.35	0.16	1.8
Cyclohexyl acetate	4.9	−0.39	−0.40	0.04	1.0

The differences between the density profiles derived from models 1 and 2 are a consequence, in part, of the fact that ellipsometry is unable to distinguish between a narrow, deep notch in the density profile and a broad and shallow density deficit.

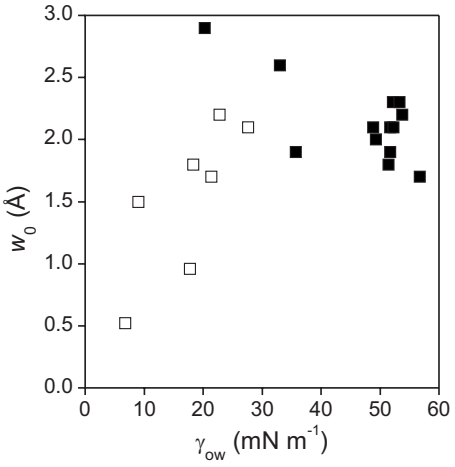

FIG. 9. Separation between oil and water phases w_0 calculated using model 2 as a function of interfacial tension γ_{ow} for a series of polar (□) and nonpolar (■) oils.

We now place our results in the context of previous experimental studies of water at solid hydrophobic interfaces and oil interfaces. The interaction of water with hydrophobic monolayers on solid substrates is closely related to the interaction of water with hydrophobic liquids. Mao *et al.* [34] have taken ellipsometric measurements on the interface between water and hydrophobic silicon and found that their results disagreed with a model of bulk water adjacent to the solid. To fit their data, a uniform drying film ($\varepsilon=1$) would have to be 0.4 Å thick—in quantitative agreement with our measurements and with the excluded volume of the hydrophobic surface. They rationalized their result by invoking the presence of "nanobubbles" of air on the solid as have been observed by atomic force microscope (AFM) [35]. They did, however, find similar disagreement for measurements at the interface between hexane and hydrophobic silicon, where nanobubbles have not been observed.

Neutron reflectivity from the interface between D_2O and perdeuterated polystyrene spin-coated onto silicon showed a region of reduced scattering length density at the interface which was interpreted as a depleted layer 20–50 Å thick acting as a precursor to the formation of nanobubbles [36]. A similar study on the interface between water and hydrophobic self-assembled monolayers on gold also noted an extended region of water at the interface (~40 Å thick) with a density of ~85–90 % compared to pure water [37]. The presence of an interfacial depleted layer in hydrophobic nanochannels of mesoporous silica approximately 6 Å thick has been invoked to explain the reduced pore volume available to water in comparison to nitrogen gas [38]. Depletion layers of this magnitude are not consistent with our ellipsometric measurements on liquid hydrocarbon-water interfaces. Recent synchrotron x-ray reflectivity results by Mezger *et al.* [39] and Poynor *et al.* [40] of the interface between water and octadecylsilane monolayers show an electron density deficit at the interface that is 2–4 and 1–6 Å thick, respectively.

Conversely, Jensen *et al.* measured the x-ray reflectivity from a water surface covered by a solid monolayer of hexatriacontane [41]. They inverted the reflectivity curves to obtain an electron density deficit at the interface of 1 Å, a value that is well described by the electron density deficit at a methyl-terminated alkane (Fig. 7). Reflectivity measurements of water covered in solid monolayers of the long-chain alcohol 1-triacontanol and the saturated triglycerides mono-, di-, and tripalmitoyl glycerol ester gave no electron density deficit. In addition to the results presented above, we have also measured the ellipticity of the interface between water and glyceryl trioleate, an unsaturated triglyceride molecule that remains a liquid at room temperature. The experimental ellipticity was -0.60×10^3 in comparison to the capillary-wave prediction from Eq. (4) of -0.38×10^3: this is the only oil we have measured that gave an ellipticity more negative than the capillary wave prediction. The behavior of glycerol trioleate is consistent with Jensen's results with the saturated analogue, glycerol tripalmitate, with the small negative deviation from the capillary-wave prediction suggesting a slight optical anisotropy at the interface. Further experiments are planned to test this possibility.

Beaglehole measured the ellipticity of the heptane-electrolyte and carbon tetrachloride-electrolyte interfaces and observed the sign of the ellipticity was opposite to that required by capillary-wave theory, in agreement with our more recent results [8]. He observed that the discrepancy between the capillary-wave prediction and the experimental result was larger for heptane than for carbon tetrachloride and suggested that the heptane chains may be structuring at the interface. Our results with a range of hydrocarbons, including octane, suggest that such structuring is unlikely to be a major contributor to $\bar{\rho}$.

Recently, Mitrinovic *et al.* carried out a detailed x-ray reflectivity study of the oil-water interface for eight linear alkanes from hexane to docosane [3]. They modeled the reflectivity curves with a hybrid model of the interface with an intrinsic interfacial width, σ_0 roughened by capillary waves, and based upon the error function profile, given by

$$\langle\rho(z)\rangle = \frac{1}{2}(\rho_1+\rho_2)+\frac{1}{2}(\rho_1-\rho_2)\mathrm{erf}\left(\frac{z}{\sqrt{2}\sigma}\right). \qquad (11)$$

The single fitting parameter σ was interpreted as the sum of a capillary-wave contribution as defined in Eq. (10a) and an intrinsic interfacial width σ_0 such that $\sigma^2=w_c^2+\sigma_0^2$. The addition of an intrinsic width to the capillary-wave thickness leads to a broadened density profile but one that always gives a permittivity intermediate between that of the alkane and water. Such monotonic profiles will always give a more negative ellipticity than the capillary-wave prediction and Mitrinovic's model is therefore not a good starting point for explaining our ellipsometry data. Nevertheless, it is worth noting that Mitronovic was able to rationalize his results with a consistent physical model without invoking any drying layer at the oil-water interface. The same model had been used to fit neutron reflectivity from the hexadecane-water interface with the same conclusion as with x-ray reflectivity—no interfacial drying [42].

V. CONCLUSION

The coefficient of ellipticity $\bar{\rho}$ for light reflected from the interface between oil and water is of the opposite sign to that expected for a sharp interface roughened by capillary waves. The values of $\bar{\rho}$ for a series of linear, branched, and cyclic alkanes, as well as unsaturated oils were not strongly dependent on molecular architecture. We conclude that molecular packing or alignment at the interface is not the primary reason for the deviation from the capillary-wave prediction for $\bar{\rho}$. We employed a stratified layer model to interpret the ellipsometric data from which we infer the drying layer at the interface is only 0.3–0.4 Å. This result may be understood by comparison with the excluded volume between adjacent hydrocarbon layers in alkane crystals. With this model, the ellipticity of the oil-water interface can be explained entirely by the van der Waals surface of the hydrocarbons without the imposition of an additional water layer of reduced density.

We also measured $\bar{\rho}$ for a series of oils containing polar functional groups in contact with water; $\bar{\rho}$ was correlated loosely with the interfacial tension. We employed the same model as above for the polar oils and found that the drying layer decreased in thickness as the favorable interaction be-

tween the two phases increased. This interaction, parametrized by the interfacial tension, is linked to the ability of the oil phase to form hydrogen bonds with water. In conclusion, if the oil phase is able to interact strongly with the water phase and form hydrogen bonds, then the drying layer thickness is reduced. To test the sensitivity of our interpretation to the model used, we also analyzed our data with a model similar to that used in x-ray and neutron reflectivity. This model gave a separation between the midpoints of the water and oil density profiles of 2–3 Å for nonpolar oils, with a reduced separation for polar oils. Though the density deficit is still small and the qualitative trends with polarity are the same in both models, the quantitative difference between the thickness of the drying layer in the two models highlights the need for care in the treatment of capillary-wave roughening.

ACKNOWLEDGMENTS

We thank the BBSRC and Unilever (Colworth) for support of this work.

APPENDIX: INTERFACIAL WIDTH VIA A COUPLED-MODE THEORY OF THERMAL FLUCTUATIONS

We follow the formalism of [22]. An infinitely thin, sharp interface with no bending rigidity ($K=0$) is modulated by a spectrum of capillary waves driven by thermal energy. The mean square amplitude of the roughness w_c^2 is given by

$$w_c^2 = \sum_q \langle \zeta_q^2 \rangle, \tag{A1}$$

where ζ_q is the amplitude of the mode of wave vector q. Employing a mode-coupling theory, the mean square amplitude of mode q is given by Meunier as

$$\langle \zeta_q^2 \rangle = \frac{1}{A} \frac{k_B T}{\Delta\rho g + \gamma(q) q^2}, \tag{A2}$$

where $\Delta\rho$ is the density difference between the adjacent phases, g is the acceleration due to gravity, $\gamma(q)=\gamma+aq^2$, $a=3k_BT/8\pi$, and A is the area of the interface. Converting the summation in Eq. (A1) into an integral over q space, one obtains

$$w_c^2 = \frac{k_B T}{2\pi} \int_{q_{\min}}^{q_{\max}} \frac{q dq}{\Delta\rho g + \gamma q^2 + a q^4}. \tag{A3}$$

The integration limits are defined by the longest and shortest wavelengths that the interface can support. In practice, ellipsometry is insensitive to capillary wavelengths longer than λ as these waves will scatter the light in an off-specular direction and will not be detected in a specular reflection experiment. This restriction places a lower limit of $q_{\min}=2\pi/\lambda$. $q_{\max}=2\pi/L_{\min}$, where $L_{\min}$ is of the order of a molecular length. Consequently, the $\Delta\rho g$ term is negligible over the range of q of interest and the integral simplifies to

$$w_c^2 \approx \frac{k_B T}{2\pi} \int_{q_{\min}}^{q_{\max}} \frac{dq}{\gamma q + a q^3} = \frac{k_B T}{2\pi\gamma} \left[\ln\left(\frac{q}{\sqrt{\gamma + a q^2}} \right) \right]_{q_{\min}}^{q_{\max}}. \tag{A4}$$

Making the reasonable assumptions that $aq_{\min}^2/\gamma \ll 1$ and $aq_{\max}^2/\gamma \gg 1$ the integrand simplifies to Eq. (A5).

$$w_c^2 = \frac{k_B T}{4\pi\gamma} \ln\left(\frac{\gamma}{a q_{\min}^2} \right) = \frac{k_B T}{4\pi\gamma} \ln\left(\frac{2\gamma\lambda^2}{3\pi k_B T} \right). \tag{A5}$$

This derivation assumes that the interface has no rigidity—this approximation has been used successfully in the study of air-liquid interfaces. To approximate the effect of a nonzero bending modulus, we note that in the independent mode approximation the variation of the ellipticity is proportional to $K^{-1/2}$ and that if the interface does have a bending modulus, the constant a is replaced by the bending modulus in Eq. (A3) [22]. Therefore for a rigid interface, the ellipticity is effectively reduced by a factor $(a/K)^{1/2}$. In the absence of ordered surfactant layers, K is typically $<k_BT$, whereas $a=3k_BT/8\pi$. The bending modulus of the interface will reduce somewhat the roughness contribution to the ellipticity, but cannot change its sign.

[1] J. S. Rowlinson and B. Widom, *Molecular Theory of Capillarity* (Dover, Mineola, N.Y., 2002).
[2] K. Lum, D. Chandler, and J. D. Weeks, J. Phys. Chem. B **103**, 4570 (1999).
[3] D. M. Mitrinovic, A. M. Tikhonov, M. Li, Z. Huang, and M. L. Schlossman, Phys. Rev. Lett. **85**, 582 (2000).
[4] A. Zarbakhsh, J. Bowers, and J. R. P. Webster, Meas. Sci. Technol. **10**, 738 (1999).
[5] M. M. Knock, G. R. Bell, E. K. Hill, H. J. Turner, and C. D. Bain, J. Phys. Chem. B **107**, 10801 (2003).
[6] M. G. Brown, D. S. Walker, E. A. Raymond, and G. L. Richmond, J. Phys. Chem. B **107**, 237 (2003).
[7] W. H. Steel, Y. Y. Lau, C. L. Beildeck, and R. A. Walker, J. Phys. Chem. B **108**, 13370 (2004).
[8] D. Beaglehole, J. Phys. Chem. **93**, 2004 (1989).
[9] A. Kereszturi and P. Jedlovsky, J. Phys. Chem. B **109**, 16782 (2005).
[10] J. P. Nicolas and N. R. de Souza, J. Chem. Phys. **120**, 2464 (2004).
[11] H. A. Patel, E. B. Nauman, and S. Garde, J. Chem. Phys. **119**, 9199 (2003).
[12] J. L. Rivera, C. McCabe, and P. T. Cummings, Phys. Rev. E **67**, 011603 (2003).
[13] S. Senapati and M. L. Berkowitz, Phys. Rev. Lett. **87**, 176101 (2001).
[14] P. Ball, Nature (London) **423**, 25 (2003).
[15] D. Chandler, Nature (London) **437**, 640 (2005).
[16] L. R. Pratt and A. Pohorille, Chem. Rev. (Washington, D.C.) **102**, 2671 (2002).
[17] R. M. A. Azzam and N. M. Bashara, *Ellipsometry and Polar-*

ized Light (North-Holland, Amsterdam, 1977).
[18] P. Drude, Ann. Phys. Chem. **43**, 126 (1891).
[19] J. Lekner, *Theory of Reflection* (Martinus Nijhoff Publishers, Dordrecht, The Netherlands, 1987).
[20] H. Bercegol, F. Gallet, D. Langevin, and J. Meunier, J. Phys. (Paris) **50**, 2277 (1989).
[21] D. Beaglehole, J. Physiol. Suppl. (Paris) **44**, C10 (1983).
[22] J. Meunier, J. Phys. (Paris) **48**, 1819 (1987).
[23] D. A. Tonova and A. A. Konova, Thin Solid Films **397**, 17 (2001).
[24] A. Hirtz and G. H. Findenegg, J. Phys.: Condens. Matter **8**, 9541 (1996).
[25] W. C. Bigelow, D. L. Pickett, and W. A. Zisman, J. Colloid Sci. **1**, 513 (1946).
[26] S. R. Goates, D. A. Schofield, and C. D. Bain, Langmuir **15**, 1400 (1999).
[27] J.-W. Benjamins, B. Jonsson, K. Thuresson, and T. Nylander, Langmuir **18**, 6437 (2002).
[28] D. E. Aspnes, Thin Solid Films **89**, 249 (1982).
[29] K. R. Mecke and S. Dietrich, Phys. Rev. E **59**, 6766 (1999).
[30] R. C. Weast, *Handbook of Chemistry and Physics* (CRC Press, Boca Raton, 1981).
[31] D. E. Small, *The Physical Chemistry of Lipids* (Plenum, New York, 1985).
[32] Q. Lei and C. D. Bain, Phys. Rev. Lett. **92**, 176103 (2004).
[33] P. W. Atkins, *Physical Chemistry* (Oxford University Press, Oxford, 1994).
[34] M. Mao, J. Zhang, R.-H. Yoon, and W. A. Ducker, Langmuir **20**, 1843 (2004).
[35] J. W. G. Tyrrell and P. Attard, Phys. Rev. Lett. **87**, 176104 (2001).
[36] R. Steitz, T. Gurberlet, T. Hauss, B. Klosgen, R. Krastev, S. Schemmel, A. C. Simonsen, and G. H. Findenegg, Langmuir **19**, 2409 (2003).
[37] D. Schwendel, T. Hayashi, R. Dahint, A. Pertsin, M. Grunze, R. Steitz, and F. Schreiber, Langmuir **19**, 2284 (2003).
[38] R. Helmy, Y. Kazakevich, C. Ni, and A. Y. Fadeev, J. Am. Chem. Soc. **127**, 12446 (2005).
[39] M. Mezger, H. Reichert, S. Schoder, J. Okasinski, H. Schroder, H. Dosch, D. Palms, J. Ralston, and V. Honkimaki, Proc. Natl. Acad. Sci. U.S.A. **103**, 18401 (2006).
[40] A. Poynor, L. Hong, I. K. Robinson, S. Granick, Z. Zhang, and P. A. Fenter, Phys. Rev. Lett. **97**, 266101 (2006).
[41] T. R. Jensen, M. Ostergaard Jensen, N. Reitzel, K. Balashev, G. H. Peters, K. Kjaer, and T. Bjornholm, Phys. Rev. Lett. **90**, 086101 (2003).
[42] A. Zarbakhsh, J. Bowers, and J. R. P. Webster, Langmuir **21**, 11596 (2005).
[43] D. L. Lide, *Handbook of Chemistry and Physics* (CRC Press, Boca Raton, 1993).
[44] H. Kalall, F. Kohler, and P. Suejda, J. Chem. Eng. Data **37**, 133 (1992).
[45] G. Korosi and E. Kovats, J. Chem. Eng. Data **26**, 323 (1981).
[46] A. Schneider, R. W. Warren, and E. J. Janoski, J. Am. Chem. Soc. **65**, 5365 (1964).
[47] F. M. Fowkes, J. Phys. Chem. **84**, 510 (1980).
[48] J. E. Shewmaker, C. E. Vogler, and E. R. Washburn, J. Phys. Chem. **58**, 945 (1954).
[49] F. L. Riddle and F. M. Fowkes, J. Phys. Chem. **112**, 3259 (1990).
[50] R. Stephenson and J. Stuart, J. Chem. Eng. Data **31**, 56 (1986); R. Stephenson, J. Chem. Eng. Data **37**, 80 (1992).